Inorganic Chemistry

Article

pubs.acs.org/IC

Magnetic Structure and Electromagnetic Properties of LnCrAsO with a ZrCuSiAs-type Structure (Ln = La, Ce, Pr, and Nd)

Sang-Won Park,[†,⊥] Hiroshi Mizoguchi,[‡] Katsuaki Kodama,[§] Shin-ichi Shamoto,[§] Toshiya Otomo,[∥] Satoru Matsuishi,[†] Toshio Kamiya,[†] and Hideo Hosono*[,†,‡]

[†]Materials and Structures Laboratory, Tokyo Institute of Technology, 4259 Nagatsuta, Midori-ku, Yokohama 226-8503, Japan

[‡]Frontier Research Center, Tokyo Institute of Technology, 4259 Nagatsuta, Midori-ku, Yokohama 226-8503, Japan

[§]Quantum Beam Science Directorate, Japan Atomic Energy Agency, Tokai, Ibaraki 319-1195, Japan

[∥]Institute of Materials Structure Science, High Energy Accelerator Research Organization (KEK), Tsukuba, Ibaraki 305-0801, Japan

Supporting Information

ABSTRACT: We report the synthesis, structure, and electromagnetic properties of Cr-based layered oxyarsenides LnCrAsO (Ln = La, Ce, Pr, and Nd) with a ZrCuSiAs-type structure. All LnCrAsO samples showed metallic electronic conduction. Electron doping in LaCrAsO by Mn-substitution for the Cr sites gave rise to a metal−insulator transition. Analysis of powder neutron diffraction data revealed that LaCrAsO had G-type antiferromagnetic (AFM) ordering, i.e., a checkerboard-type AFM ordering in the CrAs plane and antiparallel spin coupling between the adjacent CrAs planes, at 300 K with a large spin moment of 1.57 μ_B along the *c* axis. The magnetic susceptibility of LaCrAsO was very small (on the order of 10^{-3} emu/mol) and showed a broad hump at ∼550 K. First-principles density functional theory calculations of LaCrAsO explained its crystal structure and metallic nature well, but could not replicate the antiparallel spin coupling between the CrAs layers. The electronic structure of LaCrAsO is discussed with regard to those of related compounds LaFeAsO and LaMnAsO.

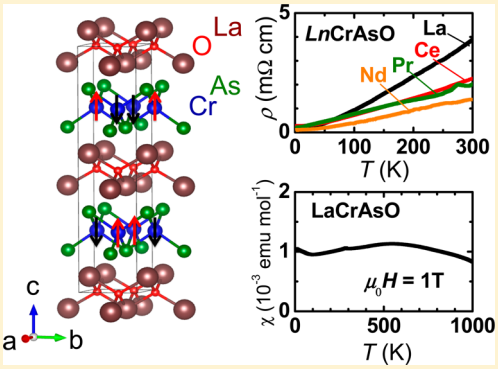

INTRODUCTION

The discovery of high-T_c iron-based superconductivity has led to intensive exploration of new classes of superconductors and the mechanisms of their superconductivity.[1,2] A common structural feature of iron-based superconductors is that they have layered crystal structures and consist of transition metals. Their family includes a wide variety of compounds with chemical formulas of, for example, $Ln^{3+}M^{2+}Pn^{3-}O^{2-}$ (Ln = lanthanide; M = transition metal; Pn = pnictogen, called 1111-type), $Ae^{2+}M^{2+}{}_2Pn^{3-}{}_2$ (Ae = alkali-earth, called 122-type), and $M^{2+}Ch^{2-}$ (Ch = chalcogen, called 11-type).[3]

Among them, the 1111-type compounds (ZrCuSiAs-type structure, space group *P*4/*nmm*) have attracted much attention because they can exhibit a variety of magnetic and electrical properties by changing the combination of the transition metal and anions even if the same crystal structure is maintained. As a result, these compounds provide a suitable playground to investigate physical properties originating from correlated electrons of 3d transition metals.[4−10] In this crystal structure, the $(Ln^{3+}O^{2-})$ blocking layer and $(M^{2+}Pn^{3-})$ layer are alternately stacked along the *c* axis. Each M ion is coordinated by four Pn ions to form an MPn_4 tetrahedron, which are connected to each other by shared edges. As M varies from Mn to Zn, the energy level of the M 3d band generally shifts to deeper energy as the effective core charge of the M ion increases, resulting in the systematic alternation of covalency between M 3d and Pn *n*p. First-principles electronic structure calculations indicate that the MAs layer is the source of the varied properties of the LnMAsO system, which implies that regulating the filling of the 3d band is one way to control electron transport and interaction, leading to a variety of physical properties in these compounds. For example, although LaFeAsO does not exhibit a superconducting transition, substitution of O sites with F and Fe sites with Co causes electron doping into the FeAs layer. This induces a phase transition from a weak antiferromagnetic (AFM) metallic state to a paramagnetic (PM) two-dimensional (2D) metallic state, which leads to a superconducting transition at ∼26 K.[1,2] LaNiAsO is a PM metal and shows a superconducting transition at ∼2.4 K without carrier doping.[4] In contrast, LaMnAsO is an AFM semiconductor with a Neel temperature (T_N) of ∼360 K and a band gap (E_g) of 1.2 eV, where the large exchange interaction in the Mn ion caused by Hund coupling opens the band gap and maintains the large magnetic moment of Mn.[6−8]

It is known that strong electron correlation is an origin of high T_c in cuprate superconductors; such correlation can form

Received: June 14, 2013
Published: November 8, 2013

   dx.doi.org/10.1021/ic401487q | *Inorg. Chem.* 2013, 52, 13363−13368

an AFM Mott insulating state in undoped states. As noted above, a similar trend is also found in many Fe-based layered superconductors, in particular, the 1111-type compounds. That is, undoped LaFeAsO has a weak AFM interaction and magnetic ordering, whereas LaFePO and LaNiPnO exhibit very weak spin interaction; as a consequence, doped LaFeAsO exhibits a higher T_c than those of the latter compounds. Considering these facts, we believe that an AFM compound with a strong electron correlation would be a good candidate for a high-T_c superconductor if the AFM ordering is diminished by electron or hole doping.

In this work, we focus on isostructral compounds with Cr^{2+}, LnCrAsO (Ln = La, Ce, Pr, and Nd), because the Cr^{2+} ion with a $3d^4$ electron configuration has a large magnetic moment and, consequently, these compounds show a strong electron correlation. LnCrAsO exhibited metallic electronic conduction, and electron doping was successful. However, no superconducting transition was detected in the chemical compositions examined in this study. The magnetic structure of LaCrAsO was revealed to be AFM both in the $a-b$ plane and along the c axis, where the spin-ordering structure is different from those of LaFeAsO and LaMnAsO.

EXPERIMENTAL SECTION

Synthesis. Synthesis of polycrystalline samples of LnCrAsO (Ln = La−Eu, Y) was attempted by solid-state reactions; however, only Ln = La, Ce, Pr, and Nd were successfully synthesized. First, LnAs was prepared by solid-state reaction of Ln (99.9%) with As (99.99%) at 1173 K for 10 h in an evacuated silica tube. Then, LnCrAsO was synthesized by heating a stoichiometric mixture of LnAs, Cr (99.99%), and Cr_2O_3 powders (99.99%) in an evacuated silica tube at 1273 K for 20 h. The resulting LnCrAsO powders were dark gray. F- and Mn-doping were also examined for LaCrAsO, where LaF_3 (99.9%) and Mn (99.9%), respectively, were used as starting reagents. We also tried to synthesize LaCrPO, LaCrSbO, and LaVAsO; however, formation of these phases was not observed.

Structure Analyses. The crystal structures of the synthesized materials were examined by powder X-ray diffraction (PXRD; Bruker D8 ADVANCE TXS) using Cu Kα radiation. PXRD data suitable for structure refinement of LaCrAsO were collected at 300 K with Debye−Scherrer optics (Bruker D8 ADVANCE; anode: sealed Mo X-ray tube with 50 kV and 50 mA) equipped with an incident beam Ge 220 monochromator, which filters Mo Kα_1 radiation only (λ = 0.71073 Å). The powder sample was sealed in a glass capillary with a diameter of 0.5 mm. The capillary was rotated continuously about its long axis during data collection to average out the preferential orientation effect. Structure refinements were performed with the Rietveld method using TOPAS4 software (Bruker AXS).[11] For LaCrAsO, time-of-flight neutron powder diffraction (TOF-NPD) data were measured to determine its magnetic parameters at room temperature (RT). The data were collected with an exposure time of 5 h at NOVA (beamline BL21, a decoupled liquid hydrogen moderator) using a 120 kW spallation neutron source at the Japan Proton Accelerator Research Complex (J-PARC), Japan. Rietveld refinements of the TOF-NPD patterns were performed using the general structure analysis system (GSAS) code.[12] The used scattering lengths of La, Cr, As, and O were 8.24×10^{-13}, 3.64×10^{-13}, 6.58×10^{-13}, and 5.80×10^{-13} cm, respectively. Elemental compositions were determined using an electron-probe microanalyzer (EPMA, JEOL, Inc. model JXA-8530F) equipped with a field-emission-type electron gun and wavelength dispersive X-ray detectors. The micrometer scale compositions in the main phase were probed on focal points 40 times, and the results were averaged.

Electrical and Magnetic Properties. The electrical resistivity of the samples was measured by the standard four-probe method in the temperature range from 2 to 300 K. Magnetization measurements were performed with a vibrating sample magnetometer (Quantum Design, PPMS) from 2 to 1000 K under a magnetic field (H) of 1 T.

DFT Calculations. DFT periodic calculations were performed for LaCrAsO with the Vienna ab initio simulation package code[13] using the generalized gradient approximation (GGA) Perdew−Burke−Ernzerhof functional,[14,15] and the projected augmented plane-wave method.[16] The crystal structure parameters obtained by the PXRD Rietveld refinements were used as initial values, and then the cell edges and internal ionic coordinates were optimized so as to achieve the minimum total energy. Several different spin configurations were examined; one was a ferromagnetic (FM) configuration with both of the two Cr ions in the unit cell. The others were AFM configurations where the two Cr ions in a CrAs plane are coupled AFM with a checkerboard (CB)- or stripe (ST)-type configuration. Interplane coupling was examined by comparing interplane FM and AFM configurations. GGA+U calculations were performed using the simplified rotationally invariant approach of Dudarev et al.,[17] where two empirical parameters, the Coulomb parameter U and the exchange parameter J, are required but treated as one independent parameter (effective Coulomb parameter) $U_{eff} = U - J$, for each localized orbital. U_{eff} was fixed at 0 eV for Cr 3d and 11.0 eV for La 4f.[18] Structural relaxation calculations were also performed at the GGA+U level, and the relaxed structures were compared with those obtained by Rietveld refinement.

RESULTS

Crystal and Magnetic Structure of LaCrAsO. As shown in Figure 1a, a clear PXRD pattern assignable to the tetragonal phase of LaCrAsO was obtained. The pattern also reveals that the sample includes the small amount of impurity phases of La_2O_3 and CrAs. Rietveld refinement confirmed that the crystal structure of LaCrAsO is of a ZrCuSiAs-type structure with the space group $P4/nmm$ (No. 129), which is illustrated in Figure 1c. Structure parameters and representative bond lengths for this crystal structure are summarized in Tables 1 and 2, respectively. The elemental compositions determined by EPMA, normalized by the molar content of Cr, were 1.04(1) for La, 0.97(1) for As, and 0.99(2) for O. The variation of the experimental reported unit cell volume for LaMAsO (M = Cr−Zn) is also shown in Figure S1 (Supporting Information) for comparison. The site symmetry of the Cr ion in LaCrAsO is D_{2d}, and the deviation from T_d symmetry is estimated from the deviation of the As−Cr−As angle from 109.47°, indicating that the $CrAs_4$ tetrahedron is elongated slightly along the c axis compared with a regular tetrahedron. The Cr^{2+} ion with a $3d^4$ electronic configuration is known to be a Jahn−Teller ion, but our results indicate that this effect is not significant for the local coordination structure. The nearest Cr−Cr distance within the CrAs layer is 2.86 Å, which is far longer than that in Cr metal (2.51 Å)[19] because of the indirect bond with intervening As. LnCrAsO (Ln = Ce, Pr, and Nd) were also successfully synthesized. PXRD measurements confirmed that each crystal structure of LnCrAsO (Ln = Ce, Pr, and Nd) is of ZrCuSiAs type. The impurities in LnCrAsO samples are summarized in Table S1 (Supporting Information). Unit cell volumes and lattice constants are presented in Figure S2 (Supporting Information).

Figure 1b shows the NPD patterns measured for LaCrAsO at RT. Table 1 summarizes the refined structural parameters, and its spin-ordering structure is drawn superimposed in Figure 1c, as indicated by arrows. The obtained structural parameters agree well with those obtained from the PXRD measurements, with a maximum difference of less than 0.1%. We first extracted the magnetic scattering contribution from the NPD pattern. Clear magnetic Bragg peaks were confirmed at wave vectors Q

dx.doi.org/10.1021/ic401487q | Inorg. Chem. 2013, 52, 13363−13368

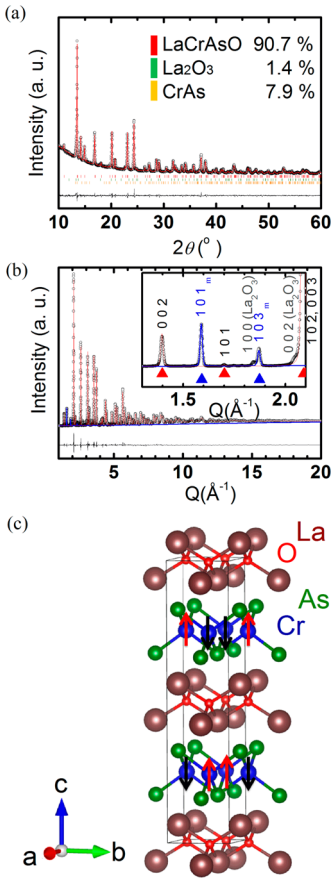

Figure 1. Crystal and magnetic structure of LaCrAsO at RT. (a, b) PXRD and TOF-NPD patterns and the simulation results obtained by Rietveld refinement. The amounts of La_2O_3 and CrAs phases estimated by the PXRD Rietveld method are 1.4 and 7.9 mol %, respectively. The NPD simulation pattern (here, $Q = 2\pi/d$) is separated into nuclear and magnetic scattering contributions (shown as red and blue lines, respectively). (c) Crystal and magnetic structure of LaCrAsO, where the arrows indicate the directions of Cr 3d spins. The magnetic unit cell, $a\times a \times 2c$, is also shown.

of 1.59 and 1.87 $Å^{-1}$, which are not indexed by integers with the original unit cell dimensions (a = 4.04 Å, c = 8.99 Å) in Table 1. In contrast, a double superlattice structure along the c axis (c = 17.97 Å) indexes them by integers as 101_m and 103_m (subscript m indicates the magnetic unit cell). No $00l°_m$ ($l°$ = odd integer) diffractions were detected, which is consistent with the extinction rule originating from the 4_2 screw axis along the c axis. The double superlattice structure along the c axis is induced by the magnetic ordering in which the Cr spins order antiparallel between the adjacent CrAs layers. To determine the spin configuration in the $a-b$ plane, we examined three different configurations: (i) FM, (ii) CB-type AFM, and (iii) ST-type AFM. The best fitting results were obtained for the CB-type AFM model (i.e., G-type magnetic ordering). Judging from the ratio between the intensities of $10l°_m$ diffractions, the spin moments are directed parallel to the c axis as illustrated in Figure 1c. The calculated effective magnetic moment of Cr was 1.568(4) μ_B/Cr, which is much smaller than the value expected from the high-spin configuration in the localized spin scheme (4 μ_B/Cr), but much larger than that expected from the low-spin configuration (0 μ_B/Cr).

Physical Properties of LaCrAsO. Figure 2a shows electrical resistivities (ρ) of LnCrAsO as a function of temperature (T) from 2 to 300 K. ρ in each sample decreased with T, consistent with metallic-type conduction. The ρ value of LaCrAsO at 300 K is 3.8×10^{-3} Ω·cm, which is of the same order of magnitude as those of the isostructural metallic compounds LaFeAsO (~6.6×10^{-3} Ω·cm) and LaNiAsO (3.5×10^{-3} Ω·cm) but higher than that of LaCoAsO (2.3×10^{-4} Ω·cm).[1,4,5]

Figure 2b and Figure S3 (Supporting Information) show the $\chi-T$ curves for LnCrAsO at an applied magnetic field $\mu_0 H$ = 1 T. The small peak at ~280 K, which was observed in magnetic susceptibility (χ)$-T$ data for the LaCrAsO sample (Figure 2b), is attributed to the AFM ordering transition of the impurity CrAs detected by PXRD and NPD measurements.[20] We confirmed that the $\chi^{-1}-T$ plot for Ln = La did not follow the Curie–Weiss law well. While weak magnetism, or Pauli PM was observed, the $\chi-T$ curve exhibited a broad maxima at 520–570 K ($T\chi_{max}$), suggesting that the system is 2D AFM.

Crystal Structures and Physical Properties of Doped LaCrAsO [LaCrAs($O_{1-x}F_x$) and La($Cr_{1-x}Mn_x$)AsO]. We successfully synthesized F-doped LaCrAsO [LaCrAs($O_{1-x}F_x$), $0 < x < 0.2$] and Mn-doped LaCrAsO [La($Cr_{1-x}Mn_x$)AsO, $0 < x < 1$]. The powder XRD patterns of LaCrAs($O_{1-x}F_x$) and La($Cr_{1-x}Mn_x$)AsO samples are shown in Figure S4a,b, respectively (Supporting Information). The formation of solid solutions was confirmed by the systematic evolution of unit cell volume, as shown in Figure S5 (Supporting Information). For LaCrAs($O_{1-x}F_x$), ρ increased monotonically with T, and decreased with increasing content of F (Figure 3a). This result is explained by electron doping because of substitution of the divalent O^{2-} ion with a monovalent F^- ion. For La($Cr_{1-x}Mn_x$)-AsO, however, electrical conductivity ($\sigma = \rho^{-1}$) decreased monotonically with increasing Mn content and exhibited a metal–insulator transition at $x \sim 0.2$ (Figure 3b). The

Table 1. Crystallographic Parameters of LaCrAsO at RT Obtained by Rietveld Refinement of PXRD and NPD Data. Data Obtained from DFT Calculations Are Also Shown for Comparison

		a (Å)		c (Å)		V (Å^3)		
XRD[a]		4.0412(3)		8.9863(7)		146.76(2)		
NPD[b]		4.04800(1)		8.9863(1)		147.252(2)		
DFT		4.10887		9.10361		153.6945		
atom	Wyckoff position	x	y	z (XRD)	B_{iso} (Å^{-2}) (XRD)	z (NPD)	B_{iso} (Å^{-2}) (NPD)	z (DFT)
La	2c	1/4	1/4	0.1365(1)	0.61(3)	0.1366(1)	0.18(1)	0.1395
Cr	2b	3/4	1/4	1/2	0.84(5)	1/2	0.57(4)	1/2
As	2c	1/4	1/4	0.6625(2)	0.83(6)	0.6628(1)	0.67(2)	0.6577
O	2a	3/4	1/4	0	0.7(2)	0	0.27(3)	0

[a] R_{wp} = 2.70%, R_p = 3.18%, and goodness of fit S = 1.60. [b] R_{wp} = 7.52%, R_p = 5.48%, and goodness of fit S = 1.20.

dx.doi.org/10.1021/ic401487q | Inorg. Chem. 2013, 52, 13363–13368

Table 2. Selected Interatomic Distances and Bonding Angles for LaCrAsO at RT

	d_{La-O} (Å)	d_{Cr-As} (Å)	As−Cr−As angles α (deg)	As−Cr−As angles β (deg)
XRD	2.364(1) × 4	2.494(1) × 4	108.26(8)	110.08(6)
NPD	2.366(1) × 4	2.497(1) × 4	108.19(5)	110.11(4)
DFT	2.415 × 4	2.506 × 4	109.15	110.11

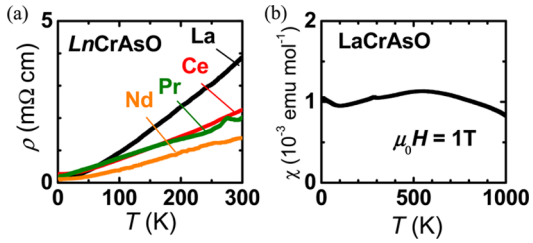

Figure 2. Temperature dependence of (a) electrical resistivity (ρ) for LnCrAsO (Ln = La, Ce, Pr, and Nd), and (b) magnetic susceptibility (χ) for LaCrAsO at 1 T.

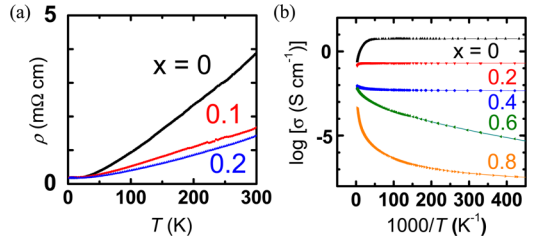

Figure 3. (a) $\rho-T$ curves for $LaCrAs(O_{1-x}F_x)$, and (b) $\sigma-T$ curves for $La(Cr_{1-x}Mn_x)AsO$.

activation energy E_a from the $\sigma-T$ data for $x = 0.6$ was about 1 meV, which indicates the opening of the band gap. Although we expected emergence of superconductivity by carrier doping of LaCrAsO as described in the Introduction, no superconducting transition was seen in either of the samples.

DFT Calculation and Band Structure of LaCrAsO. It was found experimentally that LaCrAsO is a quadratic AFM metal and forms a G-type spin configuration with a magnetic moment of 1.57 μ_B/Cr along the c axis at RT. We performed DFT calculations to understand the origin of the structural and physical properties of LaCrAsO. First, the most stable crystal and magnetic structures were examined by comparing the total energy E_{tot} for different spin configurations, i.e., (i) a non-spin-polarized calculation (no magnetism), (ii) FM spin configuration, (iii) CB-type AFM in plane/FM between planes (CB/F), (iv) CB-type AFM in plane/AFM interplane (CB/A), (v) ST-type AFM in plane/FM interplane (ST/F), and (vi) ST-type AFM in plane/AFM interplane (ST/A) (Figure 4). All of the cell edges and unit cell volumes obtained from the structure relaxation calculations agree with those determined by the corresponding Rietveld refinement within errors of 1.5%. This result shows that the CB/A (G-type AFM) and CB/F configurations have very similar E_{tot} values and are most stable for the ground state, which explains the experimental in-plane spin configuration well. It also indicates that the interplane spin interaction is very weak and should be PM; i.e., the calculations do not explain the experimental interplane AFM result. We considered that unintentional carrier doping caused by off-stoichiometry was the origin of this discrepancy and performed similar calculations for doped LaCrAsO (i.e., the total number of electrons in the unit cell was varied); however, all of these calculations gave the same result of very weak interplane spin

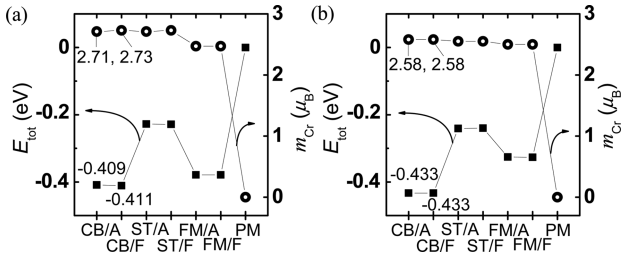

Figure 4. Total energy E_{tot} (filled squares) and Cr spin moment, m_{Cr} (open circles) calculated by DFT for LaCrAsO with different spin configurations for (a) experimental crystal structures, and (b) relaxed structures. E_{tot} represents difference values with respect to the non-spin-polarized (i.e., PM) energy and are expressed in eV per formula unit (i.e., per Cr atom). The notation for the magnetic order is as follows: PM denotes non-spin-polarized; otherwise, the first letter denotes the in-plane magnetic order (FM for ferromagnetic, ST for stripe-chain antiferromagnetic-like spin of LaFeAsO, and CB for checkerboard nearest-neighbor antiferromagnetism), and the second denotes either antiferromagnetic stacking (A) or ferromagnetic stacking (F) along the c axis.

interaction. We speculate that incorporation of a more advanced electron correlation is necessary to explain the experimental spin configuration of LaCrAsO. The spin moment of Cr is calculated to be 2.6 μ_B, which is larger than that obtained by NPD Rietveld analysis (1.568(4) μ_B/Cr at RT). The smaller experimental value is a result of thermal fluctuation at RT, similar to LaMnAsO.[7]

To determine if CrAs layers serve as conductive layers, DFT calculations were performed for LaCrAsO. Figures 5 and 6a show an $E-k$ diagram, the total density of states (DOS), and orbital/spin projected densities of states (PDOSs) of As 4p, Cr

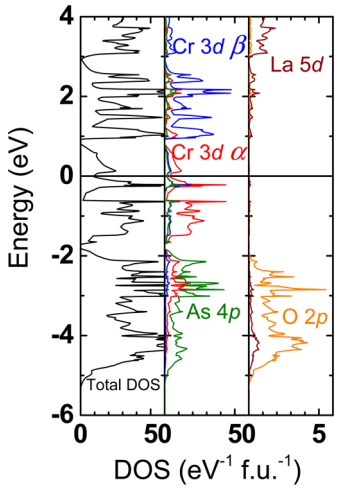

Figure 5. Total DOS (black) and PDOSs for Cr 3d (α (red) and β (blue) spin states), As 4p (green), La 5d (wine), and O 2p (orange) orbitals calculated using the CB/A configuration with the experimental structure determined at RT from PXRD data. U_{eff} was fixed at 11.0 eV for La 4f and 0 eV for Cr 3d.

dx.doi.org/10.1021/ic401487q | Inorg. Chem. 2013, 52, 13363−13368

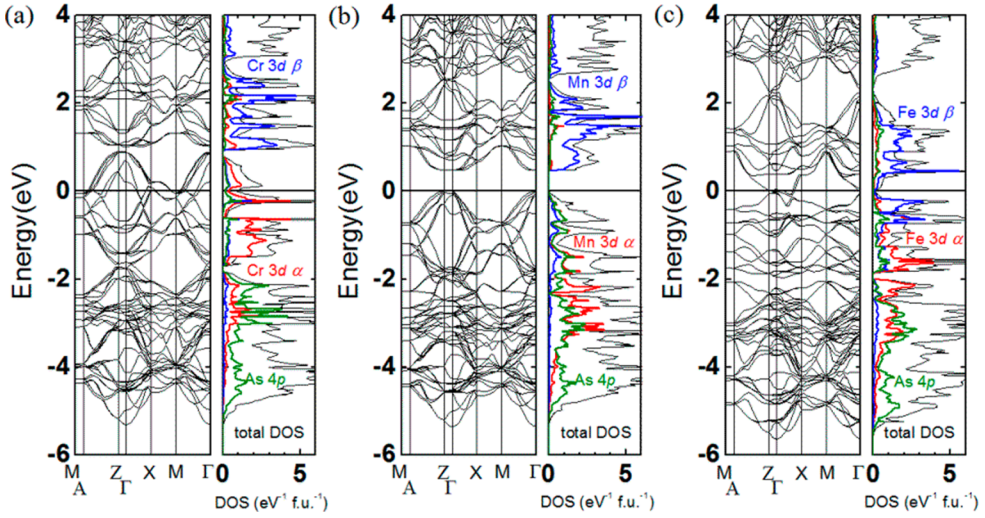

Figure 6. Comparison of band structures and DOSs for (a) LaCrAsO, (b) LaMnAsO, and (c) LaFeAsO. A $\sqrt{2}a \times \sqrt{2}a \times 2c$ supercell containing eight chemical formula units was used.

3d (up), and Cr 3d (down) around the Fermi energy (E_F) of LaCrAsO with a G-type magnetic structure. A small, but finite, DOS exists at the E_F, indicating that LaCrAsO has a metallic electronic structure, which agrees with the metallic conduction observed in Figure 2a. The electronic states around E_F are composed of highly hybridized orbitals of Cr 3d and As 4p. La 5d and 4f orbitals are located at the high energy region of 3−8 eV, and are mostly unoccupied, which is consistent with the La^{3+} valence state. O 2p states are located in the deep region of −2 to −5 eV, indicating that the LaO layers do not contribute to the electronic conduction and form a "blocking layer". The $E-k$ diagram presented in Figure 6a shows that most of the bands are almost flat along the symmetry lines ZΓ and AM, which are along the c direction. No bands crossed E_F along ZΓ, and the Fermi surface is cylindrical, indicating a 2D metallic state, as seen in LaFeAsO.

DISCUSSION

First, we discuss the magnetic interaction observed in AFM metallic LaCrAsO. The magnetic interactions between the Cr 3d spins can be classified into two categories. One is direct exchange interaction between adjacent Cr ions. The other is a superexchange interaction via an intervening As ion. It is known that elementary Cr with a body-centered cubic structure exhibits AFM/spin-density wave character with T_N = 280 K derived from direct exchange interaction.[21] When we take the much longer d_{Cr-Cr} value of LaCrAsO (2.86 Å) than that of Cr (2.51 Å) into consideration, the direct exchange interaction would not be dominant. In contrast, the DOS calculated by DFT indicated that Cr 3d orbitals are highly hybridized with As 4p to form broad bands; therefore, it is plausible that the covalent superexchange interaction dominates the magnetic character of the CrAs layer. The $\chi-T$ data for LaCrAsO show a broad halo around $T\chi_{max} \sim 550$ K, indicating 2D-AFM. However, we cannot discuss the exact Neel temperature (T_N) further because it is known that T_N and $T\chi_{max}$ can differ considerably for compounds with 2D nature, as observed for a similar 2D-AFM compound, K_2NiF_4 (T_N = 97 K and $T\chi_{max} \sim$ 250 K).[22] Nevertheless, it is expected that T_N is within 300−550 K, because LaCrAsO has a magnetic structure at 300 K (Figure 1a).

Second, we compare LaCrAsO and LaMAsO (M = Mn, Fe). The observed spin configuration of LaCrAsO is different from that of LaMnAsO where interlayer coupling is PM and that of LaFeAsO where the Fe spin moments are parallel to the $a-b$ plane with ST-type AFM configuration in the FeAs layer. Figure 6 compares the band structures and DOSs for LaMnAsO and LaFeAsO. We can see that the band structures of LaCrAsO and LaMnAsO are very similar around E_F if we consider that the E_F shift is caused by the different numbers of 3d electrons in Cr and Mn. This observation indicates that the band structure of LaCrAsO follows the rigid-band scheme and suggests that the carrier concentration of LaCrAsO may be controlled by the substitution with Mn into Cr sites, which explains the experimental $\sigma-T$ data in Figure 3b. Conversely, the band structure of LaFeAsO differs from those of LaCrAsO and LaMnAsO. A major reason for this is that Cr and Mn ions are highly spin-polarized and the band gaps open because of large Hund splitting between the up- and down-spin 3d states, whereas Fe ions are not strongly spin-polarized, as seen in the spin PDOS depicted in Figure 6c. The smaller band gap (by ∼0.1 eV) of around 1.0 eV for LaCrAsO originates from the decrease of exchange energy from Mn to Cr. However, the decrease of electrons in the 3d band gives rise to a metallic electronic state because of the E_F shift.

Finally, we briefly discuss the similarity of LaCrAsO to compounds possessing a CrAs layer. Recently, Singh and co-workers reported the electronic structure of $BaCr_2As_2$ with 122-type.[23] Its physical properties and electronic structure are very similar to those of LaCrAsO. According to their DFT calculations, the energy difference between different interlayer configurations (E_{mag} = −0.382 eV for CB/F, and E_{mag} = −0.394 eV for CB/A) was very small, although $BaCr_2As_2$ is expected to adopt a G-type magnetic structure. Taking into consideration the relatively short interlayer distance between each CrAs layer along the c axis (6.80 Å for $BaCr_2As_2$, and 8.99 Å for LaCrAsO), the energy difference in LaCrAsO is expected to be smaller than that of $BaCr_2As_2$, and our result of DFT calculations were so. Because details of the physical properties of $AeCr_2As_2$ have not been reported yet, elucidation of the interlayer interaction in compounds with a CrAs layer will be our next focus.

dx.doi.org/10.1021/ic401487q | Inorg. Chem. 2013, 52, 13363−13368

CONCLUSIONS

We presented the crystal and magnetic structure of Cr-based layered oxyarsenides LaCrAsO determined by X-ray and neutron powder diffraction measurements. LnCrAsO (Ln = La, Ce, Pr, and Nd) were successfully synthesized by solid-state reactions. Magnetic and electrical property measurements revealed that LaCrAsO is a metal with a G-type magnetic structure with the Cr spin parallel to its c axis. Itinerant AFM similar to that of LaFeAsO, which is the parent compound of Fe-based high T_c superconductors, was observed for LaCrAsO, but its magnetic order differed, with a high magnetic moment of 1.57 μ_B at RT. The temperature dependence of magnetic susceptibility of LaCrAsO also showed a broad hump at ∼550 K, indicating AFM with a Neel temperature below 550 K. Metal−insulator transition was observed for LaCrAsO upon electron doping by Mn-substitution of the Cr sites.

ASSOCIATED CONTENT

Supporting Information

Tables listing impurities and fitting parameters for LnCrAsO and figures showing variation of cell volume for LaMAsO; variation of cell edges and volumes for LnCrAsO, $LaCrAs(O_{1-x}F_x)$, and $La(Cr_{1-x}Mn_x)AsO$; temperature dependence of magnetic susceptibility for LnCrAsO; and powder XRD patterns of $LaCrAs(O_{1-x}F_x)$ and $La(Cr_{1-x}Mn_x)AsO$. This material is available free of charge via the Internet at http://pubs.acs.org.

AUTHOR INFORMATION

Corresponding Author

*E-mail: hosono@msl.titech.ac.jp.

Present Address

[⊥]Advanced Functional Thin Films Department, Korea Institute of Materials Science, Changwon, 641-831, Republic of Korea.

Notes

The authors declare no competing financial interest.

ACKNOWLEDGMENTS

This work was supported by the Funding Program for World-Leading Innovative R&D on Science and Technology (FIRST), Japan. We thank Prof. H. Hiramatsu for help with XRD measurements.

REFERENCES

(1) Kamihara, Y.; Watanabe, T.; Hirano, M.; Hosono, H. *J. Am. Chem. Soc.* **2008**, *130*, 3296.

(2) Sefat, A. S.; Huq, A.; McGuire, M. A.; Jin, R.; Sales, B. C.; Mandrus, D.; Cranswick, L. M. D.; Stephens, P. W.; Stone, K. H. *Phys. Rev. B* **2008**, *78*, 104505.

(3) Johnston, D. C. *arXiv.org, e-Print Arch., Condens. Matter* **2010**, arXiv:1005.4392.

(4) Watanabe, T.; Yanagi, H.; Kamihara, Y.; Kamiya, T.; Hirano, M.; Hosono, H. *J. Solid State Chem.* **2008**, *181*, 2117.

(5) Yanagi, H.; Kawamura, R.; Kamiya, T.; Kamihara, Y.; Hirano, M.; Nakamura, T.; Osawa, H.; Hosono, H. *Phys. Rev. B* **2008**, *77*, 224431.

(6) Kayanuma, K.; Hiramatsu, H.; Kamiya, T.; Hirano, M.; Hosono, H. *J. Appl. Phys.* **2009**, *105*, 073903.

(7) Emery, N.; Wildman, E. J.; Skakle, J. M. S.; Mclaughlin, A. C.; Smith, R. I.; Fitch, A. N. *Phys. Rev. B* **2011**, *83*, 144429.

(8) Marcinkova, A.; Hansen, T. C.; Curfs, C.; Margadonna, S.; Bos, J.-W. G. *Phys. Rev. B* **2010**, *82*, 174438.

(9) Kayanuma, K.; Kawamura, R.; Hiramatsu, H.; Yanagi, H.; Hirano, M.; Kamiya, T.; Hosono, H. *Thin Solid Films* **2008**, *516*, 5800.

(10) Yanagi, H.; Watanabe, T.; Kodama, K.; Iikubo, S.; Shamoto, S.; Kamiya, T.; Hirano, M.; Hosono, H. *J. Appl. Phys.* **2009**, *105*, 093916.

(11) *TOPAS*, Version 4; Bruker AXS: Karlsruhe, Germany, 2005.

(12) Larson, A. C.; Von Dreele, R. B., *General Structure Analysis System (GSAS)*; Los Alamos National Laboratory Report LAUR 86-748; Los Alamos National Laboratory: Los Alamos, NM, 2004.

(13) Kresse, G.; Furthmüller, J. *Phys. Rev. B* **1996**, *54*, 11169.

(14) Perdew, J. P.; Burke, K.; Ernzerhof, M. *Phys. Rev. Lett.* **1996**, *77*, 3865.

(15) Perdew, J. P.; Burke, K.; Ernzerhof, M. *Phys. Rev. Lett.* **1997**, *78*, 1396.

(16) Blöchl, P. E. *Phys. Rev. B* **1994**, *50*, 17953.

(17) Dudarev, S. L.; Botton, G. A.; Savrasov, S. Y.; Humphreys, C. J.; Sutton, A. P. *Phys. Rev. B* **1998**, *57*, 1505.

(18) Ueda, K.; Hosono, H.; Hamada, N. *J. Phys.: Condens. Matter* **2004**, *16*, 5179.

(19) Hull, A. W. *Phys. Rev.* **1921**, *17*, 571.

(20) Watanabe, H.; Kazama, N.; Yamaguchi, Y.; Ohashi, M. *J. Appl. Phys.* **1969**, *40*, 1128.

(21) Fawcett, E. *Rev. Mod. Phys.* **1988**, *60*, 209.

(22) (a) Srivastava, K. G. *Phys. Lett.* **1963**, *4*, 55. (b) Birgeneau, R. J.; Guggenheim, H. J.; Shirane, G. *Phys. Rev. B* **1970**, *1*, 2211. (c) De Jongh, L. J.; Miedema, A. R. *Adv. Phys.* **1974**, *23*, 1.

(23) Singh, D. J.; Sefat, A. S.; McGuire, M. A.; Sales, B. C.; Mandrus, D.; VanBebber, L. H.; Keppens, V. *Phys. Rev. B* **2009**, *79*, 094429.